BABEŞ-BOLYAI UNIVERSITY
FACULTY OF BIOLOGY AND GEOLOGY
DOCTORAL SCHOOL OF INTEGRATIVE BIOLOGY

THE CYANOBACTERIAL PHYCOBILISOME: STRUCTURAL AND FUNCTIONAL INVESTIGATIONS

~ SUMMARY OF DOCTORAL THESIS ~

PhD candidate
Alin Sebastian PORAV

Scientific supervisor
Prof. Dr. Nicolaie DRAGOŞ

Cluj-Napoca,
2020

Table of contents

List of abbreviation

AmAC - ammonium acetate
APC - allophycocyanin
ATP - adenosine triphosphate
ATPS - aqueous two-phase system
Bchl - bacteriochlorophyll
CBB - Calvin-Benson-Bassham cycle
CCD - couple charge device
Chl - chlorophyll
cryo-EM - cryogenic electron microscopy
cryo-EM - SPA – cryo-EM Single Particle Analysis
CTF - contrast transfer function
D_PBS - dissociated phycobilisome (s)
ddH_2O - double distillated water
DDD - direct electron detector device
DNP - H detection and dynamic nuclear polarization
DQE - detective quantum efficiency
EADS - evolution associated difference spectrum
EAFS - evolution associated fluorescence spectrum
EET - excitation energy transfer
EMDB - Electron Microscopy Data Bank
FAD – flavin adenine dinucleotide
F-ATP-ase - ATP synthase
FNR - Ferredoxin NADP Reductase
FSC - Fourier shell correlation curve
FMO - Fenna–Matthews–Olson complex
FWHM - full width at half maximum
G_PBS – PBS purified by gradient centrifugation
GTA - glutaraldehyde
IRF - instrument response function
K - partition coefficient
KPI - potassium phosphate buffer
Lcm - core membrane linkers
LHA - light harvesting antennas
LH-I - light harvesting complex I
LH-II - light harvesting complex II
LP - linker polypeptide
Lc - core linker
Lcm - core-membrane linker
Lr - rod linker
Lrc - rod-core linker
MAS - fast-magic angle spinning
MCA - multichannel analyzer
MRA - 2D multi-reference alignment
MWCO - molecular weight cutoff
NADP - nicotinamide adenine dinucleotide phosphate
NCC - Normalized cross correlation
NM - white-light probe beam in the nonlinear crystal NMR - nuclear magnetic resonance
NS - negative staining
OCP - orange carotenoid protein
OEC - oxygen evolving complex
P - purity
PBS – phycobilisome (s)
PC - phycocyanin
PCB - phycocyanobilin
PE - phycoerythrin
PEB - phycoerythrobilin
PEC - phycoerythrocyanin
PGA - 3-phosphoglyceric acid
Pf - purification factor

PQ - plastoquinone
PQH - coupling plastoquinol
PLC - plastocyanin
PSI - photosystem I
PSII - photosystem II
PSC - Perovskite solar cells
PUB - phycourobilin
PVB - phycobiliviolin
QA - primary quinone
RC - reaction centers
RCI - type I reaction center
RCII - type II reaction center
Re - recovery efficiency
RE_PBP - recovery efficiency of total phycobiliprotein
Rg - radius of gyration
RMSD - root-mean-square deviation
RMSF - root-mean-square fluctuation
ROS - reactive oxygen species
RuBP - ribulose-1,5-bisphosphate
SDS-PAGE - sodium dodecyl sulphate polyacrylamide gel electrophoresis
SEC - size exclusion column
SEM - scanning electron microscope
SNR - signal to noise ratio
Spx - spirilloxanthin
SQ - Sockley-Queisser limit
TAC - time-to-amplitude converter
TCSPC - time-correlated single photon counting
TEM - transmission electron microscope
TMHs - transmembrane helices
Vr - volume ratio
WL - white light

Keywords: cyanobacterial phycobilisome, cryo-electron microscopy, single particle reconstruction, macromolecular complex structure, macromolecular dynamics, ultrafast spectroscopy

Chapter I. General introduction

Global warming is one of humanity's most pressing problems to be solved in the 21st century. This phenomenon can be defined as an increase in average temperatures over the globe at the combined levels of atmosphere and sea surface. The earth's atmosphere, from prehistorical time, has acted like a greenhouse to capture the heat from the Sun, thus ensuring a positive temperature compatible with the occurrence and evolution of life on Earth. Even though this is not a new phenomenon in the geological history of the Earth, being reported several glacial events, the present trend of warming is of particular significance due to the rapid rate with which it takes place. Thus, the average temperature of the earth surface in 2017 has increased by almost 1 degree Celsius above the pre-industrial era, mostly because of anthropogenic activities and emissions (World Bank Group, 2020). One of the key pillars recognized by the European Union as essential for achieving the status of a climate-neutral society is the renewable energy. Today, around 40% of energy in Europe is coming from renewable energy, mainly solar and off-shore wind. By implementing the Green Deal strategy, the EU assumes that more than 80% of the total energy used by the mid-century will come from renewable energy. According to the Shockley-Queisser (SQ) limit (radiative efficiency limit), the efficiency of present photovoltaic solar cells is very close to their theoretical yield. Overcoming the Shockley-Queisser barrier and improving conversion efficiency of conventional solar cells is not a trivial task, one possible solution can be provided by Nature (Scholes, 2011). One of the most efficient mechanisms to harness the Sun power is the photosynthesis, a complex metabolic mechanism developed in nature over billions of years.

Oxygenic photosynthesis is the fundamental process responsible for all life on earth, ensuring both the organic compounds, synthesized from water and atmospheric CO_2, using light as driving energy, and oxygen as byproduct of the same reaction set. This process can be defined as a metabolic one, in which solar energy is captured and stored by an organism, which will use this energy to power all cellular processes **(**Blankenship, 2002**)**. Oxygenic photosynthesis appeared early in Earth history, approximately 3 billion years ago, and had a major impact, changing all the energetic processes of life. To better understand the importance of this process, one has to understand that most of our food and energy resources were developed using the solar energy captured during photosynthesis. The principle of this process is quite simple, namely, absorption of light energy by a molecule of chlorophyll and generation of a transmembrane pH gradient that is used as a driving force to synthesized the universal energetic molecule of living cells, namely adenosine triphosphate (ATP) (Xiong & Bauer, 2002).

The first and probably the most limiting step of photosynthesis, regardless of type, is harvesting and transferring the solar energy to the reaction centers. In this process that takes place in highly specialized pigment-protein complexes, solar energy is captured and subsequently funneled with high speed (1-100 ps) to the reaction centers. The entire process relies on unidirectional electron energy transfer within a network of chromophores (pigments) with the final target being the special pair of chlorophyll from the core of the reaction centers (Croce et al., 2018). The shape, size, energy gap, and absorption strengths of chromophores determines how apoproteins modulates the interactions between them. Light harvesting can be seen as a two-step process, where, firstly, solar photons are absorbed by molecular chromophores, which stores the energy in an electronic excited state, followed by conveyance of energy, through Förster resonant energy transfer, within and among light-harvesting proteins until it reaches the target (Mirkovic et al., 2017). The main purpose of the light harvesting antenna is to expand the spectra from which the phototrophs are capable of absorbing, thereby conferring them an adaptive advantage in a constantly changing environment.

Phycobilisomes, found in cyanobacteria, red algae and glaucophyte, are the second largest LHA, after chlorosomes, with a molecular weight ranging from 1 MDa to 18 MDa and dimensions up to 68×45×39 nm. This complex is found in a variety of forms, from hemidiscoidal and hemiellipsoidal to bundle shape, and all of them can be segregated from a structural and functional point of view into two compartments, a cylindrical core from which several rods of stacked disks radiate (MacCall, 1998). The core varies in a species dependent manner, from bicylindrical and tricylindrical to pentacylindrical form, but is always made up from disks of allophycocyanin (APC) kept together by linker polypeptides. The rods are assembled from hexameric disks of phycocyanin (PC), and in some strains from both phycocyanin and phycoerythrin (PE), with the later one located distal to the PC (Adir et al., 2005). Rods are held in the assembled form and are attached to the APC core by specific linker proteins (Mullineaux, 2008). Even though structural studies of the phycobilisome were employed as early as 1960 by the groups of Gantt, Glazer and Bryant, until recently, just structures of low resolution obtained by negative staining electron microscopy were available (Yi et al, 2005; Chang et al., 2015). Zhang et al. (2017) managed to obtain the first high resolution (3.5 Å) structure of the phycobilisome from *Griffithsia pacifica* in 2017. Since then, another high-resolution structure was solved for the phycobilisome from *Porphyridium purpureum* by Ma et al., (2020). Both structures were solved for phycobilisomes from red algae, which means that the structure of cyanobacterial PBS is still unsolved at a high enough resolution, in order to allow atomic model building.

Chapter II. Aims of the thesis

The main focus of this thesis was to explore the structural features of cyanobacterial phycobilisome at near atomic resolution in order to reveal its basic architecture, thus enhancing our understanding of the basic principles that guide both the assembly process and the function of this "*giant"* macromolecular complex. We consider that successfully conducting these studies will provide novel and insightful information on how photosynthesis is harnessing solar energy.

In order to successfully accomplish this ambitious goal, we have defined five operational objectives, namely:

a) development of a suitable purification and visualization method of the cyanobacterial phycobilisomes;

b) analysis of energy transfer dynamics inside phycobilisomes;

c) identification and characterization of molecular building blocks of cyanobacterial phycobilisome;

d) phycobilisome conformational heterogeneity analysis and identification of a suitable specimen for cryo-electron microscopy analysis;

e) phycobilisome 3D structure analysis using single particle analysis cryo-electron microscopy. These objectives, were extensively addressed in dedicated chapters.

Chapter III. Phycobilisome purification and negative staining optimization

{This chapter was partially published as: Porav, A. S., Bocăneală, M., Fălămaş, A., Bogdan, D. F., Barbu-Tudoran, L., Hegeduş, A., & Dragoş, N. (2020). Sequential aqueous two-phase system for simultaneous purification of cyanobacterial phycobiliproteins. *Bioresource Technology*, *315*, 123794. doi.org/10.1016/j.biortech.2020.123794*}*

1. Introduction

Supramolecular assembly of biomolecules, also known as macromolecular complexes or molecular machines, performs a wide range of biological functions. They are assembled in an orderly manner and consist of two to several thousand individual subunits, including DNA, RNA, proteins and lipids (Scarff et al., 2018). These molecular machines are kept together by one of the two means, covalent bonds or weak protein-protein interactions, and usually undergo conformational changes to perform their function. Elucidating the structure of these nanomachines is crucial for understanding their cellular function and how cells work in both health and disease (Chang et al., 2015). From a localization point of view, these machines can be classified into three categories: soluble proteins, found in cytoplasm, subcellular organelle or in nucleus; membrane proteins, found anchored or fully embedded into various cellular membranes; and finally, proteins

associated with extracellular matrix (Beck & Baumaister, 2016). Regardless of the selected method for structural investigation, these complexes must be obtained in a highly purified state, without affecting their structure or functionality. Phycobilisomes are highly sensible complexes that are relatively stable in high ionic strength buffers based on phosphates (Gantt, 1975). Due to special buffer requirements, PBS are difficult targets for both negative staining analysis and cryo-electron microscopy. For negative staining, the major drawback is the presence in high concentration of the phosphate, which reacts strongly with uranium salts forming bulk precipitates. For cryo-EM the problem is represented by the ionic strength of the buffer (1 M) which prevents the formation of nice vitrified ice, this being similar to ice crystal and sucrose. Also, the presence in high concentration of macroelements is increasing the background noise of micrographs, making it almost impossible to identify the protein complexes. Additionally, the PBS is one of the best examples of supramolecular complexes which are biochemically pure but structurally, they present compositional variability. This is due to the overall composition of PBS being assembled from identical subunits and thus, the absence/presence of one or more identical subunits cannot be identified by standard biochemical methods, such as sodium dodecyl sulphate polyacrylamide gel electrophoresis (SDS-PAGE).

Here, we aimed to develop and optimize a methodology to investigate the structural and functional features of the cyanobacterial phycobilisomes. The optimization process followed three major steps: development of a suitable method for PBS purification, negative staining optimization and cryo-EM grid optimization.

2. Materials and methods

- We used four different cyanobacterial strains, *Arthrospira platensis* strain AICB 49, *Cronbergia* sp. strain AICB 1097, *Coelomoron pussilum* strain AICB 1012 și *Fremyella diplosiphon* strain UTEX 481. The cyanobacteria strains were acquired from the Algae and Cyanobacteria Collection of the Institute of Biological Research in Cluj-Napoca (Dragos et al., 1997). These cyanobacterial strains were chosen for these investigations, due to their phycobilisome particularities in terms of composition.
- The phycobilisomes were purified using two approaches: a) one assuming the development of an aqueous two-phase system based on potassium phosphate and PEG, and b) one using sucrose gradient centrifugation. Samples obtained by both methods were subjected to another purification step, size exclusion chromatography.
- The purity of the PBS sample and its functional integrity was investigated using SDS-PAGE and both, steady state absorption and fluorescence spectroscopy

- Negative staining procedure optimized for PBS visualization was adapted from Arteni et al. (2008) with several modifications.

3. Results and discussions

Previously, in order to explore the effectiveness of PBS purification and concentration, an aqueous two-phase system was used to study partitioning behavior of cyanobacterial phycobiliproteins. It is well known that PC tends to migrate in the PEG-rich phase while APC prefers the salt-rich phase (Patil et al., 2008). Here we bypassed the partitioning of individual PBP by maintaining the PBS in their intact form, thus concentrating and partially purifying them. For all TX-114 treated samples, the aqueous two-phase system was employed by addition of 10% solid PEG, resulting in a volume ratio of 0.7, indicating a concentrated PEG-phase (Figure III.1).

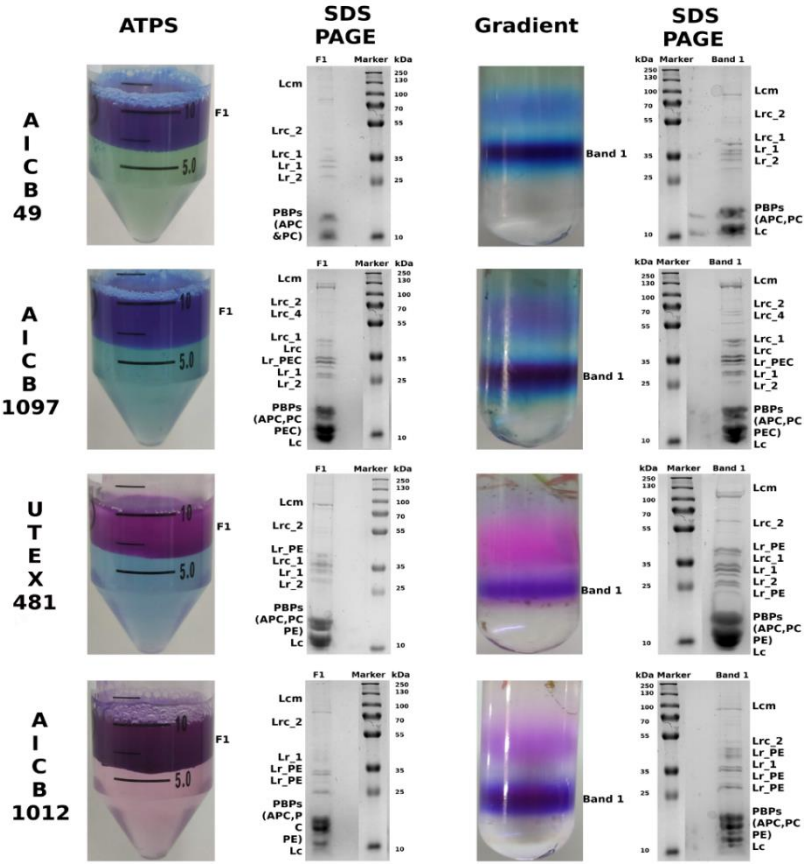

Figure III.1. Phycobilisome purification and associated SDS-PAGE profiles**.**

The parameters for designing the ATPS, such as PEG concentration, salt concentration and pH were established based on the phase diagrams found in literature (Glyk et al., 2014). In all samples, the targeted proteins showed a high affinity for the PEG-phase. The partition coefficient (K) and recovery efficiency of PBS, associated with the increase in purity, confirm that most of the PBP are found in the top phase. The recovery efficiency in *A. platensis* was higher than 97% while for *Cronbergia* it was ~92%. In both cases, the purity of total PBPs increased by a factor of

5, compared with the brute extract, and with a factor of 2 compared with TX-114 extract. The recovery and partitioning coefficient of PBS was lower in samples containing PE, with a yield of 76% for *Fremyella* while for *C. pusillum* the yield was 88%. The recovery yield of individual PBP in *A. platensis* and *Cronbergia.* showed more homogeneous results compared to the strains containing PE, suggesting that their PBS are more stable. Although, the recovery rate from *Fremyella* was lower, the analysis of individual PBP showed that both PE and PC were recovered over 90%, the low yield being a consequence of APC loss, probably due to week interactions between the core and rods of the PBSs. By comparing the purity grade of individual PBP from the ATPS_PBS samples with those of C_PBS, we determined that the contamination ratio with proteins not involved in the PBS structure is low (<10%). Gradient centrifugation is a well-established method to purify large macromolecular complexes. Similar to the ATPS, the colored layer from TX-114 treated samples were used for PBS purification. By centrifugation, the samples were partitioned in 2 to 3 layers. For AICB 49 there were two main bands, one at 1M which contained functionally active PBS and one between 0.4 and 0.8, composed mostly by individual phycobiliproteins. In case of PE and PEC containing strains, we obtained three bands, at 1.2 M, at 0.8 M, and one between 0.4 and 0.8 M. The band between and 0.4 and 0.8 was similar to the one from the previous two strains, containing mostly phycobiliproteins. The 0.8 M band is not very concentrated, making it difficult to visualize it, and is formed by partially dissociated PBS. The lowest band (1.2 M) is composed from intact PBS.

The partitioning behavior of all samples in both ATPS and gradient centrifugation is presented in Figure III.1. Also, the associated protein composition, as resolved by SDS-PAGE, is illustrated in the same figure. Negative staining is a powerful technique to analyze the protein structure and dynamics at low resolutions. Unfortunately, even though this technique is considered to be “ancient” and easy to apply, its success is specimen dependent. The conventional negative staining protocols usually follow three main steps: a) specimen adsorption on a carbon coated EM grid which was previously glow-discharged; b) grid washing on one or two drops of distillated water; c) staining with heavy metal solution. As stated before, due to peculiar properties of phycobilisomes and their special buffer requirements, the traditional negative staining protocol is not applicable. For this reason, we required to investigate and optimize an appropriate method to negative stain the PBS.

In the optimization process we pursued the influence of different methods of grid hydrophilization over the PBSs absorption and orientations; different heavy metal salts behavior and capacity to stain the PBSs without affecting their structural integrity; various methods to remove the phosphate salts; several grid types. Other experimentally determined parameters for negative staining were the exposure time required for both adsorption and staining of PBS, and

also the optimal sample concentration. Several selected results obtained during the optimization process are illustrated in Figure III.2.

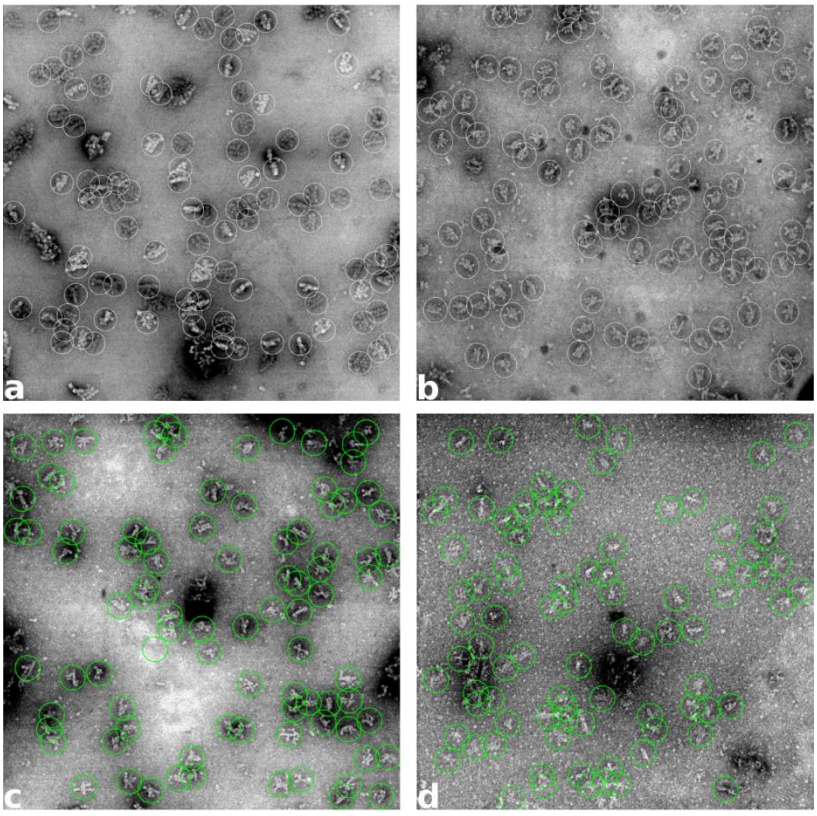

Figure III.2. Phycobilisome negative staining micrographs. a) *A. platensis* PBS; b) *Cronbergia* PBS; c) *C. pussilum* PBS; d) *Fremyella* PBS. All micrographs were acquired at 60,000x nominal magnification

4. Conclusions

In the present study, we successfully developed and optimized a method for phycobilisome analysis by negative staining electron microscopy. Even though the ATPS is a fast and good method for PBS purification, the difficulty of PEG removal makes this method unsuitable for negative staining. Addition of a final size exclusion steps to the purification improved the homogeneity of the sample by at least 30%. The negative staining procedure presented here can be applied to any specimen that is sensitive to buffer or environment conditions, not only to the phycobilisomes.

Chapter IV. Energy transfer dynamics within phycobilisomes

{This chapter was partially published as: Fălămaș, A., Porav, S. A., & Tosa, V. (2020). Investigations of the energy transfer in the phycobilisome antenna of *Arthrospira platensis* using femtosecond spectroscopy. *Applied Sciences*, *10*(11), 4045. doi.org/10.3390/app10114045*}*

1. Introduction

Photosynthesis is a crucial process, that maintains life on Earth by converting solar energy in storable chemical energy. This process occurs in phototrophic organisms such as plant, eukaryotic algae and cyanobacteria. Solar-energy conversion is highly dependent on the ability of the organism to capture and efficiently transfer the energy to the catalytic reaction centers (Blankenship, 2014). Photosynthetic organisms developed over evolutionary time different structural strategies to increase the energy availability at the reaction centers by widen their light absorption spectra and thus, their optical cross section (Croce et al., 2018). This key step in photosynthesis is performed by light harvesting antenna (LHA) systems made up of pigment-protein complexes that coordinates a large number of chromophores. LHA complexes capture and store the energy in the electronic excited states of the chromophores, which is then transferred within the complex system until it reaches the target chromophores in the reaction center (Scholes et al., 2011). Time-resolved absorption and fluorescence measurements have been employed to investigate the mechanism of energy transfer in PBP on the femtosecond (fs) to nanosecond (ns) time scale (Liu et al., 2013). Multiple theories have been proposed for the ultrafast dynamics observed in PBPs, with the most likely involving Förster energy transfer based on the energy resonant interaction of transition dipoles of donor and acceptor molecules, which can be applied for donor-acceptor distances $\geq$ 20 Å. Absorption spectra of different PBP, coincide with the excitation spectra, so pigments that absorb at lower wavelengths transfer and concentrate their energy to the pigments with higher wavelengths and low energy. This is possible only if the latter ones are at favorable distance and have the right orientation of the dipole moments.

Understanding energy transfer in phycobilisomes extracted from cyanobacteria can be useful for building biomimetic hybrid systems for optimized solar energy collection and photo-current amplification.

2. Material and methods

- We used the same biological material presented in the previous chapter.
- The integrity of the PBS samples was assessed using steady state fluorescence and SDS-PAGE.
- The energy transfer dynamics was investigated by time resolved spectroscopy using both transient absorption and time resolved fluorescence. Briefly, the samples were pumped with

580 nm femtosecond (fs) pulses obtained using an optical parametric amplifier (Orpheus, Light Conversion) from the 1030 nm pulse emitted by an Yb:KGWlaser (Pharos, Light Conversion) of 170 fs laser pulse duration and 80 kHz repetition frequency. For the transient absorption (TA) experiments (Harpia, Light Conversion), a supercontinuum probe pulse was obtained by focusing 10% of the 1030 nm pulse in a sapphire crystal. After traveling through an optical delay line, the withe light transmitted through the sample is detected using a spectrograph with 300 L/mm grating combined with an array detector. The polarization between the pump and probe pulses was set at the 54.7◦magic angle. The fluorescence kinetics was investigated using the time-correlated single photon counting (TCSPC) setup (Chimera,Light Conversion). The samples were excited with vertically polarized light, and the fluorescence emission was collected through a long-pass filter suitable for each sample emission and an emission polarizer set at the magic angle (54.7◦relative to the polarization of the pump pulse). The fluorescence signal was focused on the entrance slit of a double monochromator and detected using a single photonsensitive photomultiplier (Becker&Hickl PMC-100-1 standard). The FWHM of the instrument response function (IRF) was 340 ps. For the TCSPC experiments, the average power of the pump beam was 2 mW, while for the TA experiments, laser pulses of 3–4 mW were used.

3. Results and discussions

The fluorescence kinetics of the PBS was recorded in the 645-700 nm spectral region after the system was pumped with 580 nm laser pulses. The resulted TCSPC data are presented in Figure IV.4. The fluorescence emission spectra showed a maximum around 660 nm with a red-shift towards 670 nm for emission spectra recorded at later time moments. The fluorescence kinetics was subject to global analysis fitting, assuming a simple sequential mode. We supposed that the excitation energy was transferred between different molecular species inside the PBS among the most energetically efficient route. The fluorescence kinetics of the PBS required two spectro-kinetic components for a satisfactory fit. A short component in the range of the IRF of our system was detected and a long component of 1.77 ns. The resulted EAFS showed maxima at 655 nm and 668 nm, respectively. Additionally, the short EAFS decreased suddenly until approximately 676 nm.

The first component showed smaller amplitude compared to the second one, which could indicate smaller fluorescence yield induced by excitation energy transfer to the terminal emitter. Moreover, the maximum of the short EAFS component was observed at 655 nm and matched the fluorescence emission maximum of PC, however, it also matched the short EAFS obtained in APC. Therefore, this kinetic component may be associated to PC or to a spectral form of PCB in APC

that transfers the excitation energy to terminal emitter in APC. The peaks correspond well with the species associated spectra reported by van Stokkum et al., (2018) for the time-resolved emission spectra recorded from a wild type PBS from Synechocystis PCC 6803 at 649 and 660 nm which were assigned to PC 650 and APC 660, respectively.

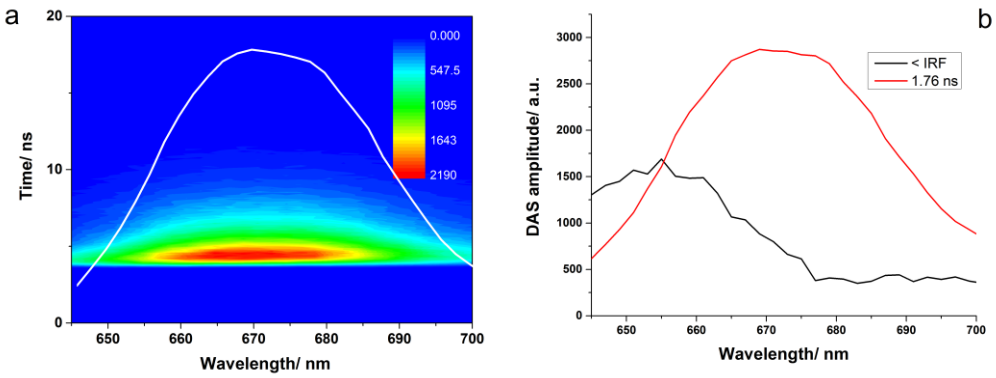

Figure IV.4. (a) 3D TCSPC data carpet recorded from the PBS (AICB 49) excited at 580 nm. The white spectrum corresponds to the steady-state fluorescence emission spectrum; (b) The EAFS obtained from global fitting analysis.

Further, we applied time-resolved absorption spectroscopy to map the energy transfer processes within our PBS sample and identify the ultrafast decay times. The time-resolved difference absorption signal was detected across a range of wavelengths from 475 to 750 nm. Figure IV.5 shows the difference absorption spectra obtained at various delay times when the PBS was excited at 580 nm. A bleaching of the ground state centred at 624 nm appeared immediately following the laser excitation, within the first 400 fs. Concomitantly, two positive absorption bands were observed, a smaller one in the 470-550 nm and a stronger one in the 650-700 nm spectral range. The latter band was already reported in the scientific literature and it was suggested that it could represent an excited state absorption of PC since it emerged together with the bleaching band (Theiss et al., 2008).

The former band decayed with dynamics similar to the bleaching band, while the latter one, however, decayed within 1-100 ps, then became negative and increased again approaching the zero line. A more recent study performed by Niedzwiedzki et al. (2019) on *Acaryochloris marina* PBS components, suggest that since the 650-700 nm positive band decays faster than the 470-550 nm one, it cannot be assigned to an excited state absorption and associated it instead to a temporary electrochromic response of phycocyanobilins that are in the ground state and in the proximity of the excited ones. After reaching its maximum, the bleaching band started to decrease and its peak shifted to 633 nm until 100 ps delay time. Similar investigations were performed on the phycobilisomes purified from other three cyanobacterial strains, namely *Coelomoron pussilum* AICB 1012, *Cronbergia* sp. AICB 1097 and *Fremyella* UTEX 481.

The limited space as well as the fact that the results obtained for the three cyanobacterial strains mentioned above were not published yet, determined us not to include the results in this summary, instead they are detailed in the extenso version of the thesis.

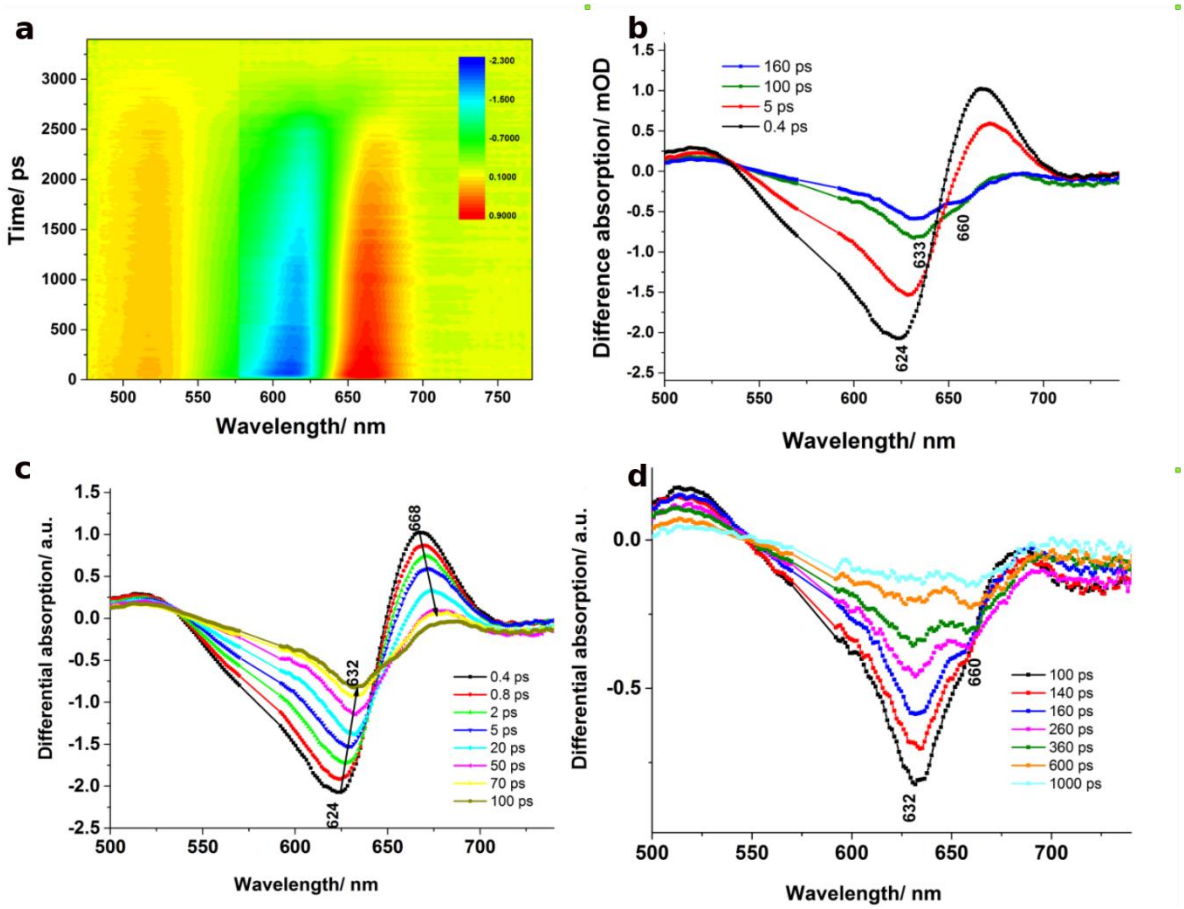

Figure IV.5. a) 3D transient absorption data carpet obtained from PBS (AICB 49) pumped at 610 nm, b) transient absorption spectra of the PBS showing the bleach recovery of the ground state; c) the evolution associated difference spectra resulted following global analysis, and d) examples of kinetic traces together with the obtained fits.

4. Conclusions

The present work describes the ultrafast kinetic and dynamics of the excitation energy transfer in the phycobilisome extracted from four cyanobacterial strains, namely *Arthrospira platensis* AICB 49, *Coelomoron pussilum* AICB 1012, *Cronbergia* sp. AICB 1097, and *Fremyella diplosphon* sp. UTEX 481. The results obtained for A. platensis are in accordance with those reported in literature for other strains of *Arthrospira platensis* and *Synechocystis* sp., which presents a similar phycobilisome composition. Additionally, here we present for the first time the dynamic behaviour of energy transfer, as probed by time resolved spectroscopy, between the PBS components of both *Coelomoron pussilum* AICB 1012 and *Cronbergia* AICB 1097. It is worth to mention that due to immensity and complexity of the phycobilisomes, there are probably many more interactions between chromophores and thus a more complex energy transfer dynamics, but due to the limitations of the existing infrastructure they cannot be segregated.

Chapter V. Phycobilisome structural components and homology modeling.

1. Introduction

Atomic models of proteins are essential for understanding the molecular mechanisms of biological processes. In the past 20 years, the number of experimentally determined structures increased exponentially from 13,589 in 2000, to more than 165,400 in 2020 (May), mostly due to technological advancement in both hardware and software (Marks et al., 2012). Even though the number of protein structures available increased substantially, the sequencing technology also evolved drastically, resulting in a huge number of sequenced genomes. As a consequence, the sequence-structure gap is increasing at a faster pace (Marks et al., 2012). To tackle this discrepancy, computational methods for predicting and modeling the 3D structure of monomeric and complex proteins were developed. The deficiency of 3D structure prediction approach is a direct consequence of the structural information available to us. Most of the structural knowledge is provided by X-ray crystallography, a technique that is able to provide only information about a single conformation that is amenable to crystallization.Even though tremendous improvements were made in the EM field, as it is a routine to reach near atomic resolutions (2-5 Å), for globular proteins and stable complexes it requires the previous knowledge of certain essential information, such as protein sequence, 2D features and even homology for building the atomic model (Elmlund & Elmlund, 2017).

The aim of this chapter was to identify all structural components of the phycobilisomes from three cyanobacterial strains (*A. platensis* AICB 49, *Cronbergia* sp. AICB 1097, *C. pussilum* AICB 1012) and to obtain their 3D structure by homology modelling. To accomplish this, we sequenced and annotated the cyanobacterial genomes, the phycobilisome associated proteins based on known proteins from literature and public databases, followed by a prediction of their structure using multiple software packages.

2. Material and methods.

- *Cyanobacteria strains*: A. *platensis* AICB 49, *Cronbergia* sp. AICB 1097 and *C. pussilum* AICB 1012 were grown as describe in chapter III subsection 2.2.1
- *Genomic DNA isolation***:** gDNA isolation was performed using ZR Soil Microprobe DNA MiniPrepTM kit (Zymo Research, Irvine, CA, USA), according to the manufacture recommended protocol. The DNA sample obtained was spectrophotometrically quantified at NanoDrop 2000 (ThermoScientific, USA).
- *Genome sequencing of cyanobacterial strains* was performed using Shotgun sequencing technique on an Illumina Novaseq 6000 platform (Novogene, HongKong, China). The raw

Illumina genomic reads (comprising between approx. 9 to 13 million sequences) were pre-processed in order to remove low-quality bases/reads and adaptor sequences using the bbmap package. The PE reads were interleaved by reformat.sh and quality trimmed by bbduk.sh (qtri =rltrimq=18) (Bushnell et al., 2016). Subsequently, bbduk.sh was used for adapter trimming and identification/removal of possible PhiX and p-Fosil2 contamination (k =21 ref=vectorfile ordered cardinality). The obtained contigs (3 datasets), with lengths higher than 2 kb, were used for protein coding genes prediction with PRODIGAL v2.6.3 (default settings).

- *Structure prediction:* The sequence of phycobilisome protein components were retrieved from the sequenced genomes and used as targets for template search. The best templates, with the highest quality score and best global identity percentage (GI), were used for modelling the three-dimensional structures with both Phyre2 server (Kelley et al., 2015) and Swiss-Model server (Waterhouse et al., 2018) using the default settings.
- The quality of protein models obtained from both servers was estimated based on the Global Model Quality Estimation (GMQE) and Qualitative Model Energy Analysis (QMEAN) statistical parameters. Also, the best model obtained for each protein was subjected to backbone analysis of torsional angles through the Ramachandran plot generated by the Rampage server.

3. Results and discussion

The structure and composition of PBPs were extensively studied during the past 25 years as evidenced by the relatively large number of structures available in PDB. As shown in Figure V.2, the homology degree between subunits of the same PBP from different species is very high. Comparing them with the available crystal structures have also shown a high structural similarity. Thus, for PBP subunits modeling we used the template 1HA7 from *A. platensis* found in PDB. All PBP subunits were modeled with 100% confidence with a coverage ranging between 95% for AICB 1012 to 100% for AICB 49. Analysis of the secondary structure of α-subunit revealed that ~60% of the structure is formed by alpha helix motifs, while the rest of the polypeptide is composed of disorder regions, usually found between the alpha helices (Figure V.1).

The β-subunit is made of six alpha helices, which together represent 70% of the protein. Similar to α-subunit, the rest of the β-subunit is represented by disordered regions. Beta-strands are missing in each subunit from each species. The most conserved regions in both subunits are the bilin binding domains. All PBP polypeptides share the same, feather-like structure, indicating a high degree of structural conservation among them.

Linker polypeptides have a crucial role in phycobilisome assembly, forming the blueprint after which the process takes place. Until recently (Zhang et al., 2017) due to their instability, there

were just a handful of experimental structures, mostly determined by X-ray or NMR spectroscopy. Also, the available structures were for the small linkers, APC and PC associated. Once with the publication of the PBS structure from *G. pacifica* by Zhang et al., 2017, the structural information about linker structures expanded, and thus facilitated the homology modeling process. We found that the PBS core from each strain studied has just one linker associated only to APC (ApcC). The 3D model was predicted using the template from *M. laminosus* code 1B33. The secondary structure made from two beta strands (24%) and two alpha helices (46%). The high percentage of disordered regions is making the structure highly flexible.

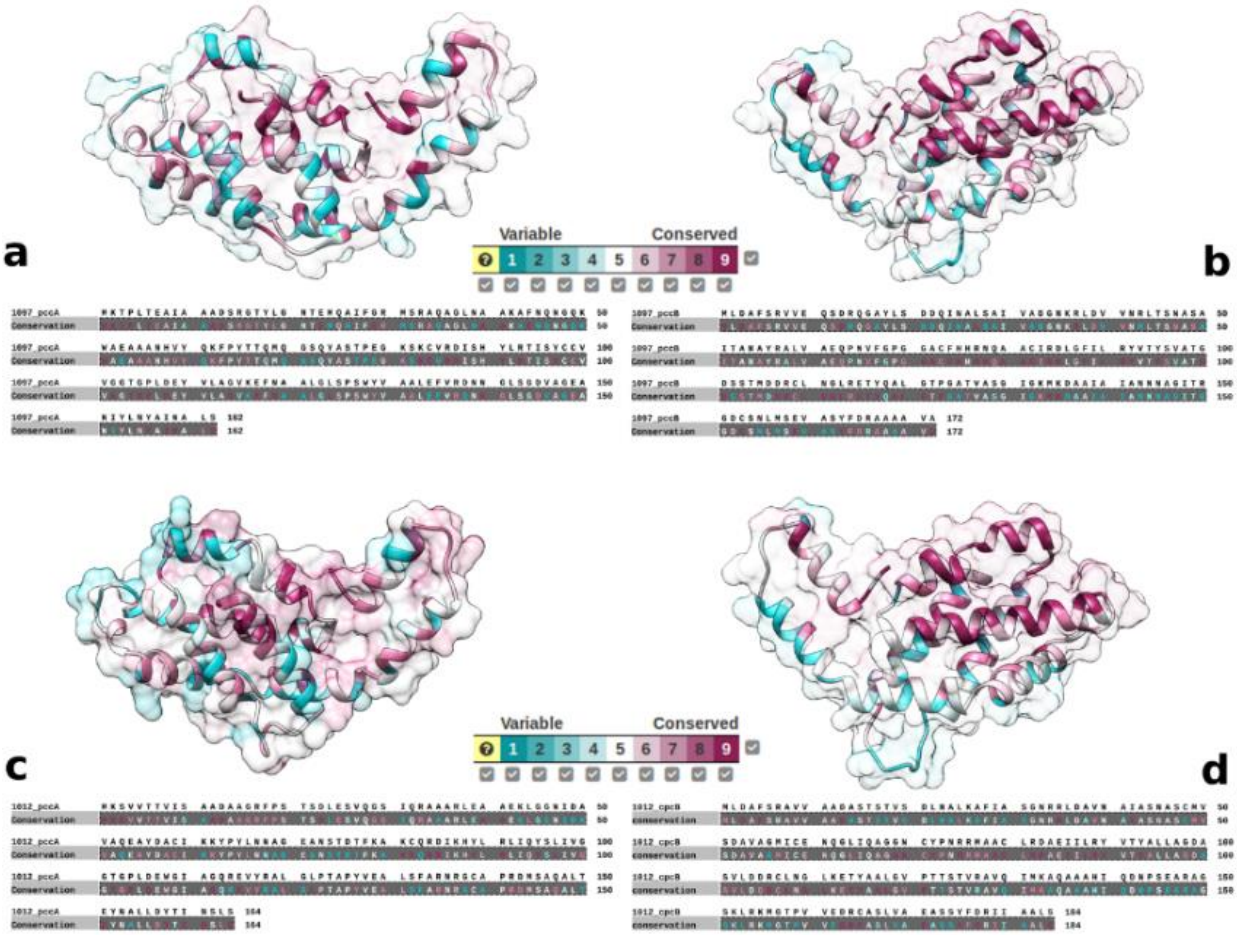

Figure V.1. 3D models of phycobiliproteins, colored by conservation degree. a) PEC α-subunit; b) PEC β-subunit; c) PE α-subunit; d) PE β-subunit

Structural composition analysis of the polypeptides revealed the presence of the pfam domain PF01383 also known as CpcD domain (Figure V.4). The small PC associated linker (CpcD2) was modeled using the same template as for apcC. Compared with the APC linker, CpcD2 has multiple beta strands (5) and just one alpha helix. Unorganized regions cover more than 50% of the entire protein. Another resemblance is the presence of the same domain (PF01383), suggesting its importance in hexameric assembling of PBPs. Large phycobiliprotein linkers were

modelled based on the templates of the linkers extracted from the PBS structure of *G. pacifica* (5Y6P) (Zhang et al., 2017) and *P. purpureum* (6KGX) (Ma et al., 2020). The sequence identity between the target proteins and templates was relatively low (~35%), but combining the templates we covered around 90% of the structure, while the rest of the protein being modelled *de novo*. Structural investigation showed a similar topology for all rod associated linkers regardless of the phycobiliprotein with which it interacts. Basically, each of them has a large PF00427 at the N-terminus part while close to C-terminal, a part of PF01383 domain is found. PC associated rod linker are found in all three cyanobacteria strain while the PEC rod linker only at AICB 1097 and PE rod linker only at AICB 1012. The same organization was found for polypeptides from each strain despite that the sequences show low identity.

4. Conclusions

Homology modeling is a powerful computational tool for analyzing the 3D structures of proteins which exploit the evolutionary restraint, that the structure suffers modifications slower than the sequence. By sequencing and assembling the genomes of the cyanobacterial strains used in this work, we identified and retrieved the sequences of each PBS components from all strains. Each strain has its own PBS particularities, despite having the same architecture. Here, we present for the first time the molecular composition of the phycobilisome from diazotrophic cyanobacteria *Cronbergia sp*. AICB 1097 and from *Coelomoron pussilum* AICB 1012. The number of unique proteins which constitutes structural components of the PBS varies among strains. Each phycobiliprotein has its unique linker polypeptides which even if they do not share a high sequence homology have an almost identical structure.Structural conservation analysis showed a high similarity degree among the PBS components from different strains.

Chapter VI. Conformational flexibility of phycobilisomes.

1. Introduction

Proteins are the building blocks of every metabolic pathway found in living cells. Fulfilment of their function is strongly related to their dynamics and capacity to interact and accommodate to both internal and external signals. Most proteins perform their specific function in association with other proteins, forming highly organized macromolecular complexes. The structural adaptation to a function can be of compositional nature or conformational nature.

Despite many attempts, that were made to solve the structure of PBS from numerous cyanobacterial and red algae strains, there are only two high resolution structures of red algae PBS available in PDB (ID:6KGX- *P. purpureum* (Ma et al., 2020), 5Y6P- *G. pacifica* (Zhang et al.,

2017), and an additional three low resolution structures of cyanobacterial PBS deposited in Electron Microscopy Data Bank (EMDB) under the following ID: EMD-2821 – *Anabaena sp.* strain PCC 7120 (Chang et al., 2015), EMD-6430- *Halomicronema hongdechloris* (Li et al., 2016) and EMD-4601 – *Synechosystis* sp. PCC 6803 (Rast et al., 2019). Paradoxical, even though the most common PBS family is the hemidiscoidal type, and thus the most studied one, the high-resolution structures available describe the block shape (5Y6P) (Zhang et al., 2017) and the hemiellipsoidal shape (6KGX) (Ma et al., 2020).Controversially, although all hemidiscoidal shape PBS present the same organizational compartments, the core and rods, the structural models proposed, based on EM analysis, are highly versatile. The 3D model diversity is not targeting only the rod number or core cylinders but also the rod distribution, the distances and angles between the rods.

In the presented context, the main goal of this chapter was the investigation of phycobilisome flexibility and its origin. To properly address this issue, we used a combination of three powerful methods used in structural analysis, namely: negative staining electron microscopy, image analysis and molecular dynamics simulation. To ensure an optimal coverage of PBS type, we chose to investigate the three cyanobacterial strains that have different PBP composition, namely *A. platensis* AICB 49, *Cronbergia* sp. AICB 1097, and *C. pussilum* AICB 1012.

2. Material and methods

- The phycobilisome sample preparation for negative staining EM analysis were performed as previously described in chapter III.
- *Image acquisition:* PBS samples were examined on a HD-2700 scanning transmission electron microscope (Hitachi High-Tech, Tokyo, Japan), operated at 200 kV. Micrographs of AICB 49 PBS were recorded with DigiscanII (Gatan Inc., Pleasanton, CA) at a size of 2048x2048 and a nominal magnification of 80k, yielding a pixel size at the sample level of 4.1 Å. Micrographs of AICB 1097 and 1012 PBS, were recorded with the same system, but at a 4096x4096 size and a nominal magnification of 60k, which resulted in a pixel size of 4 Å. For each strain, we collected 200 micrographs for screening purpose. After preliminary image analysis, we further acquired 1,100 micrographs for AICB 49.
- *Image analysis:* The micrographs were processed in the cryoSPARC (Punjani et al., 2017) software package and Relion (Scheres, 2012). The contrast transfer function (CTF) was estimated and corrected using CTFFIND4 program (Rohou & Grigorief, 2015). For each data set we manually picked 2,000 particles (around 20 micrographs) that were used to train a neural network in CrYOLO (Wagner et al., 2019). The picked particles were windowed and extracted from micrographs in 600 Å boxes. The extracted particles were subjected to several rounds of

unsupervised 2D classification in Relion, to clean the data set of artefacts, aggregated and damaged particles. The 3D classification was performed with standard settings but restricting the number of classes to five. The structure refinement was repeated for 3 times and the template was low-pass filtered to 60 Å before each refinement

- *Flexibility analysis*: The high conformational variability of the phycobilisome rods from AICB 49 determined us to evaluate the flexibility of rod-core linker proteins. The models of all rod-core linkers were subjected to flexibility analysis in CABS-flex 2.0 server (Kuriata et al., 2018). This program uses all-atom Molecular Dynamics simulations with different sets of restraints to evaluate the fluctuation of proteins and the best convergence models are reported. The configuration settings used for these simulations were SS2 mode with a gap value of 3, minimum and maximum restrains of 3 and 8 respectively. We used 100 cycles at a medium temperature value (1.4) and the trajectory frames were saved at every 10 cycles. Models showing high mobility were further investigated by long Corse Grained Molecular Dynamic using UNRES server (Czaplewski et al., 2018).

3. Results and discussions

The grids containing negatively stained PBS from AICB 49 were further subjected to a round of visual screening under the microscope, in order to identify the best samples in terms of PBS distribution and quality of the stain. In the end, two grids were selected for manually acquisition of 1,100 micrographs. Compared with the screening part, where we manually picked all the particles, here we manually picked particles from 20 micrographs and used them to train a neural network in crYOLO for automatic unassisted particle picking. By using the trained model, we obtained 95,745 particles, resulting in a mean value of 87 particles per micrographs. A cleaning scheme as in the screening step was applied with minor modification. To ensure that most of bad particles are easily distinguished and averaged together, we split the particles in ten equal stacks and performed three iterative steps of reference free 2D averaging, urging for 250 classes which render around 40 particles per class. After removing every class from each particle stack that didn't show clear protein features, the remaining particles were merged in one stack and were subjected to another cleaning step using 100 particles per class. After this procedure we discarded more than 50% of all particles, resulting a final stack of 42,420 good particles. This stack was further used for flexibility analysis.

Figure VI.1 shows the 2D classes obtained from the cleaned data set. As can be seen, several conformations are present, most of the structural variability being located at the third pair of rods. Based on the angular distribution of this rod pair, we identified four different conformations. Due to the fact that the angular variability can be observed on classes which

illustrates a side view of the PBS, only these classes were divided according to the identified conformations and merged in a single particle stack for each of the four conformations. The same procedure was applied for both bottom and prone orientation. In total we obtained 28 classes out of which 18 were different side view projection, 6 bottom view projections, and 4 represented by prone projections. Side view projections accounted for 64% of the final particle stack while the bottom and prone represented only 26% and 10%, respectively. As stated above, the side view classes were divided in four conformations (C1-4) as follows: C1: class 2, 5, 6, 18, 20, 25; C2: class 3, 8, 9, 12, 13, 15, 17; C3: 26, 27; C4: 7, 14, 28. The particles were not evenly distributed between the 4 conformations, those in the first two conformation were populated by more than 80% of the total particles representing side view projections. The weakest representation was of the third conformation, only 4%, while the fourth conformation accounts for 14%.

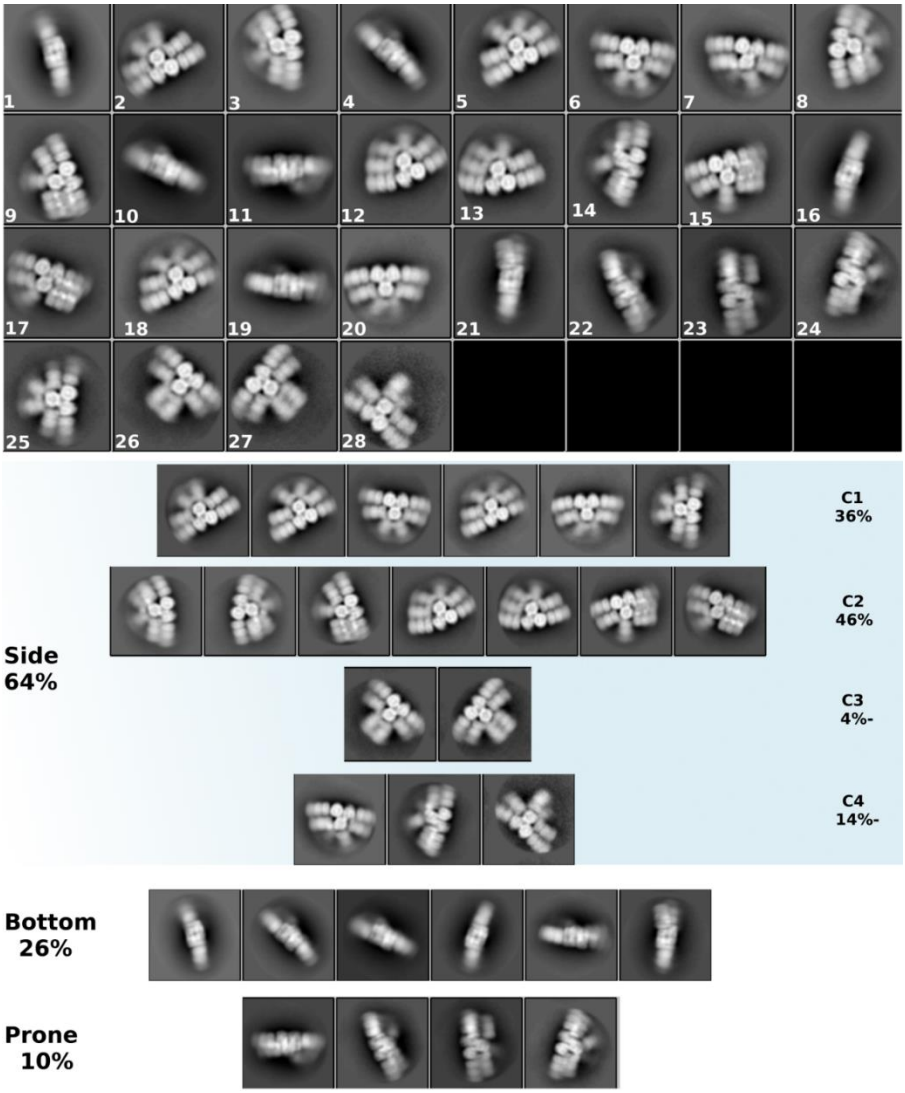

Figure VI.1. 2D class averages of AICB 49 phycobilisome representing different rod orientation. One square has 80 nm.

The highly localized flexibility at the interface between the core and the top rod pair made us postulate that one of the rod-core linkers (Lrc) identified in the genome may play a key role. This theory was reinforced by data found in literature, suggesting that phycobiliproteins have low flexibility. According to Su et al., (2017), the PC in both forms, trimeric and hexameric, have low flexibility, the residue fluctuation being around 1 Å. To properly address the flexibility problem, we used the 3D predicted structure of the rod-core linkers (CpcG) from all three strains obtained in the previous chapter (V), to perform molecular dynamic simulations by two complementary software packages, CABS-flex and UNRES. Regardless of the software used, before simulation we performed one ns energy minimization step for each protein structure. Based on molecular dynamics simulation performed here, we showed that the CpcG2 linker demonstrates higher flexibility than CpcG1 linker, in both C- and N-terminal domains.

Further, we tried to highlight the rod's flexibility in 3D by applying several rounds of heterogeneous refinement with different starting templates. For obtaining the templates illustrating different positions for the flexible rod pair, we chose the same particle sub-stacks used for highlighting the rod motion in 2D, to generate the initial models by the same *ab-initio* reconstruction process. After one round of homogeneous refinements, five 3D models were used for heterogeneous refinement of the curated particle stack that generated the above structure. Using this approach, we managed to obtain 15 PBS models, each showing a different architectural localization for the top rod pair. In some cases, the models do not exhibit full length rods, probably due to the low particle number that embraces a specific projection. However, even though the rod density is shallow, it is enough to deduce their orientation. As expected, the top rod pair of the AICB 49 PBS reveals high amplitude motion.

4. Conclusions

In the present study we used a hybrid approach, combining electron microscopy with molecular dynamics, to investigate the structural features of cyanobacterial phycobilisome. Thereby, here we present for the first time a 3D model for the classic hemidiscoidal phycobilisome from *A. platensis*. The phycobilisome from AICB 49 is characterized by a tree-cylindrical core from which six rods are radiating. Our findings showed, contrary to previous knowledge, that the PBS can adopt in the same strain several conformations due to rod flexibility. Using molecular dynamics, we confirmed that certain rod-core linkers have high flexibility, making them the perfect candidates to carry out the rod motions. Furthermore, during the screening process, we managed to establish the structural organization of the PBS from both *Cronbergia* AICB 1097 (hemidiscoidal with eight rods) and *C. pussilum* AICB 1012 (hemidiscoidal six rod PBS).

Chapter VII. Cryo-EM analysis of *Arthrospira platensis* phycobilisome

1. Introduction

The recent innovations in the cryo-EM field, transform this method from "blobology" to the "method of choice" for addressing structural features with near-atomic resolution of large and dynamic macromolecular complexes that are intangible to conventional structural techniques such as X-ray crystallography or NMR. Structure determination of such structures is essential for unlocking the secrets of key metabolic functions such as transcription, translation, splicing, electron transport, intra- and inter-cellular transport, or even photosynthesis. Usually, the photosynthetic process is performed by large supercomplexes formed by the association of photochemical reaction centers with antennae proteins. The high photosynthetic efficiency is strongly correlated with the ability of antennae proteins to harvest and supply photons to the reaction centers. The molecular mechanism of energy transfer is still unclear, despite having been studied extensively (Mirkovic et al., 2017). Most of the structural studies, that investigate light harvesting antennas (LHA) are focused on the smaller chlorophyll binding type, like those found in higher plants and anoxygenic photosynthetic bacteria.

Comprehension of the intricacy and functions of the photosynthetic complexes and supercomplexes, will ultimately help designing and constructing bio-mimetic devices that will ensure a clean and stable energy supply, thus contributing to solving one of the central challenges of the 21st century. In this chapter we aimed to investigate the structure of cyanobacterial phycobilisome at near atomic resolution by taking advantage of the advancement of cryo-electron microscopy.

2. Material and methods

- The phycobilisome sample preparation for negative staining EM analysis were performed as previously described in chapter III.
- *Cryo-EM sample preparation and data collection:* A hybrid optimized method, similar to that used for negative staining, was developed for cryo-EM single particle analysis to take into account the stability features of PBS. Briefly, a 4 µl aliquot of freshly purified PBS sample at 0.2 mg/ml concentration, was added to a glow discharged 400 mesh cooper grid with lacey carbon layer backed by an additional ultrathin continuous carbon layer. The glow discharge process was performed for 30 sec using a PELCO easiGlow™. The grid vitrification was performed with Vitrobot Mark IV (FEI Company) at room temperature and 100% humidity using a 6 s blotting time (Ash-free Whatman filter paper nr. 1), with a blot force of 6, after which the grids were plunged in liquid ethane. Vitrified grids were loaded in G2 Titan Krios (FEI Company) fitted with a FALCON III direct electron detector (Astbury Biostructure

Facility, Leeds, UK). The microscope was operated at 300 kV at a nominal magnification of 75k with the detector in the integrating mode. EPU software was used to set up a 96 h automated data collection which resulted in 13,635 micrographs at 1.065 Å/pixel. The micrographs were collected with an exposure time of 1.5 sec, a total dose of 74.4 e/Å^2 across 59 fractions which resulted in a dose per fraction of 1.26 e/Å^2. The defocus range was set between -1 and -3.5 µm.

- *Image processing:* The entire processing workflow was performed in cryoSPARC v2.15 (Punjani et al., 2017) and Relion 3.0 (Scheres, 2012; Zivanov et al., 2018) software packages unless stated otherwise. MotionCor2 (Zheng et al., 2017) was used for initial beam and drift induced motion correction, while CTF was estimated using CTFFIND4 software (Rohou and Grigorief, 2015). automated picking two approaches were used, the first one involved the training of a neural network in crYOLO (Wagner et al., 2019) and used in the same package for particle picking, while the second one implied particle picking based on 2D templates in cryoSPARC. To clean the data set of damaged particles, carbon edge, and ice crystals several reference-free 2D averages were performed. The clean data set was used for obtaining an initial 3D model using *ab initio* reconstruction. The model obtained was further used for homogeneous refinement. The final particle stack was used for another round of homogeneous refinement followed by non-uniform refinement and CTF refinement.

3. Results and discussions

Reference free 2D averaging was used for particle cleaning using a similar procedure with the one described in chapter VI under section 3.1. After three iterative 2D classification we removed most of the damaged particles by discarding poor resolved classes. The same procedure was performed on both particle stacks, template based picked (tb-stack), and crYOLO picked (cr-stack). After cleaning, the template based picked was formed by 62,135 particles, while the one picked by crYOLO had 57,526 particles after the final curation step. Further, the crYOLO stack was analyzed in RELION 3.0 and the template based in cryoSPARC v2.58. The best 2D classes obtained for the two particle stacks are presented in Figure VII.4. As can be seen, despite the number of classes generated, which is software dependent, there are no major differences between the two approaches regarding the number of particle orientation. When compared with the negative staining classes, where we managed to obtain several different conformations and thus proving the existence of flexibility, at least to some extent, in cryo 2D classes we couldn't point out different orientations for the top rod pair. Additionally, the rods of vitrified PBS seem to be formed by only 2 hexamers and not three, as the samples used for negative staining, suggesting that the PBS was purified from culture found in a different state or that the light intensity was higher. The reason for this change denotes sample preparation requirements, such as the necessity of PBS to be prepared

fresh. Thereby, the *A. platensis* AICB 49 culture from which we prepared the samples were grown at Astbury Center, thus changing the location, and with it the culture system. Even though we tried to maintain the same culture parameter it seems that the illumination intensity at the culture level was slightly higher. Another reason could be the timing of the culture state as a result of microscope time reserve, not always being free for screening.

The resolution obtained for both particle stacks is between 4.5 Å and 9.8 Å, differing among classes. As can be observed in Figure VII.4, in classes generated by both software packages, secondary structure features, like alpha helices, can be distinguished. The overall structure is identical with the one found by negative staining, presenting a tri-cylindrical core from which six rods radiate. The core structure is the most stable part of PBS, as it turns out from the 2D classes based on the highly resolved structural features observed. In the case of the rods, only one hexamer is clearly resolved, while the second PC hexamers is blurry. This is indicating that not all particles have the second PC hexamer on the rods, or that are not fully embedded in ice due to the high PBS dimensions.

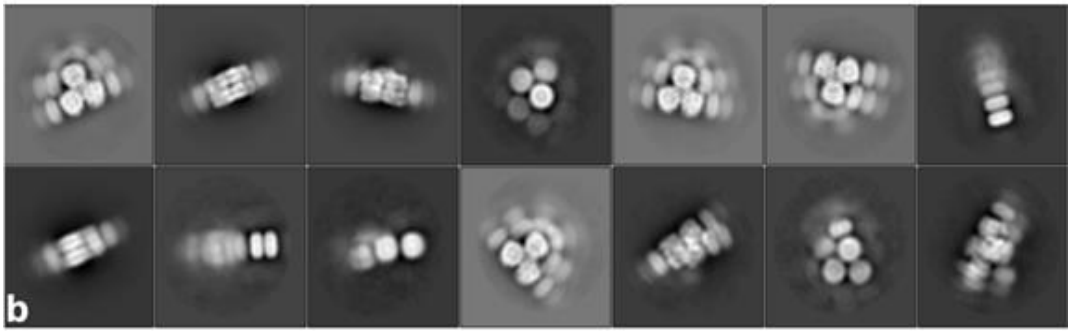

Figure VII.1. 2D class averaging.

The clean particle stack, obtained in cryoSPARC, was further used for 3D reconstructions. First, we used *ab initio* reconstruction to generate an initial 3D model of the complex. The obtained model was used as a template for 3D classification in RELION. Analyzing the 3D classes, we noticed that two out of five classes resembled the PBS structure obtained by negative staining while the other three were damaged structures. Also, the two good classes contained 82 % of the particles. To ensure homogeneity of the particle stack before performing homogeneous refinement, we repeated the 3D classification procedure, iteratively, for three more times, after each time discarding the classes depicting damaged particles. To further improve the quality of the particles we used heterogeneous refinement in cryoSPARC to sort out compositional heterogeneity. After this cleaning procedure, we discarded almost 35% of the particles used for obtaining 2D classes, the final cleaned particle stack being formed by 37,418 particles. Further analysis was performed only in cryoSPARC software package.

Non-uniform refinement without enforced symmetry resulted in a similar structure obtained by homogeneous refinement, while the C2 symmetry resulted in an overall improvement

of the structure, the final resolution being 5.14 Å (Figure VII.2). In our attempts to improve the PBS structure we performed structural refinement using different parameters regarding enforced symmetry, noise model, local and global CTF refinement, and different masks having sequential tightening degrees. From all parameters tested, only the local CTF refinement had a small positive influence over the visual quality of the structure but unfortunately without improving the nominal resolution.

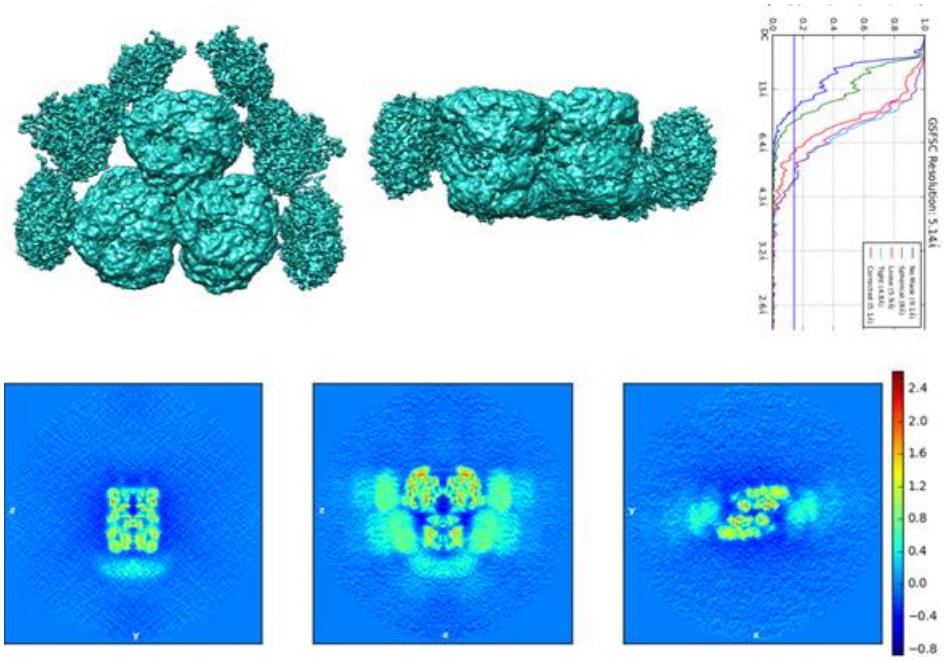

`**Figure VII.2.** Phycobilisome 3D model

The PBS 3D structure from *A. platensis* AICB 49 was reconstructed by single particle cryo-electron microscopy with a global resolution of **5.14 Å**. A closer visual inspection showed that the resolution varies a lot between regions. Thus, by calculating the local resolution, we established that the resolution is ranging from 3 Å, in the middle of the core, to 11 Å for some rod regions (Figure VII.6). This confirms the previous statement that the core is the most stable part of PBS. Due to this resolution gradient, cumulated with the fact that only one hexamer for each rod showed a suitable density, we build a minimal 3D structure for the PBS composed of tricylindrical core and six rods each with only one PC hexamer. This was considered to be the minimal structure of a fully functional PBS which presents all essential proteins. The second and third PC hexamers would be assembled on the rods in a polymerizing manner without additional functional roles compared with the first PC hexamer. Thus, the physical dimensions are smaller than what we reported by negative staining, having 356 Å in length, 275 Å height, and a thickness of approximately 140 Å. Even though the PBS from AICB 49 is one of the largest macromolecular complexes that was structurally investigated, it is smaller in terms of both size and mass when compared with the other two published structure of PBS from *G. pacifica* (Zhang et al., 2017) and *P. purpureum* (Ma et al.,2020).

4. Conclusions

In the present chapter we determined for the first time the structure of a cyanobacterial (*Arthrospira platensis*) phycobilisome at subnanometric resolution using cryo-electron microscopy coupled with single particle reconstruction. The phycobilisome sample, due to its particularities, poses some difficulties to cryo-EM analysis but they were successfully overcome, resulting in a new hybrid protocol for sample vitrification, that involves sample fixation on grid and buffer exchange without blotting. Using more than 13,000 micrographs we obtained a structure with a global resolution of **5.14** Å, which allowed us to reconstruct the minimal structure by molecular fitting. The PBS structure reconstructed here has 144 individual phycocyanobilin chromophores, and more than 170 polypeptides. The differences between PBS core organization from red algae and cyanobacteria and even between different cyanobacteria are questioning the importance of architectural plasticity in phycobilisome-photosystem interactions.

Chapter VIII. Conclusions and perspectives.

The main conclusions of the investigations presented in this thesis are the following:

- The cyanobacterial phycobilisomes are highly unstable macromolecular complexes that require high ionic strength buffers which interferes with structural analysis. The phycobilisome purification method developed here, based on aqueous two-phase system is powerful and reliable, but unfortunately is only suitable for spectroscopic analysis and not for structural investigations. This is the first time, when ATPS is used for purification of large macromolecular complexes;
- The ultrafast spectroscopy confirms that the energy transfer between phycobilisome components occurs sequentially, from the peripheral components to the core. For each strain investigated, the energy transfer process was explained using four decay times and two compartments (rod and core). As far as we know, this is the first comparative study which shows that the phycobilisome composition does not influence the energy transfer scheme, but rather alters kinetics;
- Genomic analysis revealed that the number of unique proteins involved in the structure of phytobilisomes varies between strains, being strongly correlated with their particular composition. Sequence analysis showed that individual phycobiliproteins have high degree of conservation and even when the sequence similarities between each type of phytobiliprotein are lower, they have the same feather-like, structure. Similar to the phycobiliproteins, the sequence homology of phycobilisome linker polypeptides is low but the structure is highly conserved;

- We show here, for the first time, that the large number of structural models proposed in the literature for the hemidiscoidal phycobilisome, may be a consequence of conformational flexibility. The most flexible phycobilisome was noticed to be the one from *Arthropisra platensis* AICB 49, with the highest flexible region being at the interface between the top rods and the core, suggesting a key role in rod-core linkers. Additionally, using molecular dynamics, we argued that one of the rod-core linkers from *Arthrospira platensis* has a higher motion degree than those from *Cronbergia* sp. AICB 1097 and *Coelomoron pussilum* AICB 1012;
- We present the first subnanometric structure of a cyanobacterial phycobilisome **(5.14 Å)**, namely that of *Arthrospira platensis* AICB 49. The overall structure depicts a hemidiscoidal shape with a tri-cylindrical core to which six rods are anchored. By solving the structure of the cyanobacterial phycobilisome, we were able to observe the key structural differences of the allophycocyanin core structure compared with the one from red algae. These differences are probably a consequence of the rod number anchored to the core and are presumably related to the phycobilisome-photosystem connection mechanism.

As a final remark, the results presented in this thesis provide insightful information about the structural organization and functional kinetics of cyanobacterial phycobilisome, which together with the conformational flexibility proved by molecular dynamics, outlines a complex molecular picture of light harvesting process in the early days of photosynthesis.

Nevertheless, many open questions remain unanswered regarding the light harvesting process in cyanobacteria:

- First, what is the functional significance of phycobilisome flexibility? The available data about the phycobilisome structure under different illumination regimes are scarce, thus allowing us only to make assumptions over the functional role played by flexible rods.

- Another unanswered question for which we need more structural investigations, is related to the structural conservation of the phycobilisomes during evolution. Even though we showed here that the structure of our cyanobacterial phycobilisome is the same with the minimal functional structure of those from red algae, we can't help but wonder why the phycobilisome of red algae can attach directly a phycoerythrin rods to the core.

List of publications related to the thesis

The research carried out in this PhD thesis has been partially published in the following articles:

Drulyte, I., Johnson, R. M., Hesketh, E. L., Hurdiss, D. L., Scarff, C. A., **Porav**, S. A., Ranson, N. A., Muench, S. P., & Thompson, R. F. (2018). Approaches to altering particle distributions in cryo-electron microscopy sample preparation. *Acta Crystallographica Section D: Structural Biology*, *74*(6), 560–571. (IF: 3.227)

Fălămaș*, A., **Porav***, S. A., & Tosa, V. (2020). Investigations of the energy transfer in the phycobilisomeantenna of *Arthrospira platensis* using femtosecond spectroscopy. *Applied Sciences*, *10*(11), 4045. (IF: 2.474)

Porav, A. S., Bocăneală, M., Fălămaş, A., Bogdan, D. F., Barbu-Tudoran, L., Hegeduş, A., & Dragoş, N. (2020). Sequential aqueous two-phase system for simultaneous purification of cyanobacterial phycobiliproteins. *Bioresource Technology*, *315*, 123794. (IF: 7.539)

** authors contributed equally to the manuscript*

Selective references

Adir, N. (2005). Elucidation of the molecular structures of components of the phycobilisome: Reconstructing a giant. *Photosynthesis Research*, *85*(1), 15–32. https://doi.org/10.1007/s11120-004-2143-y

Beck, M., & Baumeister, W. (2016). Cryo-Electron Tomography: can it reveal the molecular sociology of cells in atomic detail? *Trends in Cell Biology*, *26*(11), 825–837. https://doi.org/10.1016/j.tcb.2016.08.006

Blankenship, R. E. (Ed.). (2002). *Molecular Mechanisms of Photosynthesis*. Blackwell Science Ltd. https://doi.org/10.1002/9780470758472

Blankenship, R. E. (Ed.). (2014). *Molecular mechanisms of photosynthesis* (2nd ed). Wiley/Blackwell.

Cardona, T., Shao, S., & Nixon, P. J. (2018). Enhancing photosynthesis in plants: The light reactions. *Essays in Biochemistry*, *62*(1), 85–94. https://doi.org/10.1042/EBC20170015

Chang, L., Liu, X., Li, Y., Liu, C.-C., Yang, F., Zhao, J., & Sui, S.-F. (2015). Structural organization of an intact phycobilisome and its association with photosystem II. *Cell Research*, *25*(6), 726–737. https://doi.org/10.1038/cr.2015.59

Croce, R., Grondelle, R. van, Amerongen, H. van, & Stokkum, I. van (Eds.). (2018). *Light harvesting in photosynthesis*. CRC Press

Czaplewski, C., Karczyńska, A., Sieradzan, A. K., & Liwo, A. (2018). UNRES server for physics-based coarse-grained simulations and prediction of protein structure, dynamics and thermodynamics. *Nucleic Acids Research*, *46*(W1), W304–W309. https://doi.org/10.1093/nar/gky328

Dragoș, N., Péterfi, L. S., Momeu, L. & Popescu, C. (1997). *An Introduction to the Algae and the Culture* C*ollection of Algae at the Institute of Biological Research, Cluj-Napoca*. Cluj University Press

Gantt, E. (1975). Phycobilisomes: light-harvesting pigment complexes. *BioScience*, *25*(12), 781–788. https://doi.org/10.2307/1297221

Glyk, A., Scheper, T., & Beutel, S. (2014). Influence of different phase-forming parameters on the phase diagram of several PEG–salt aqueous two-phase systems. *Journal of Chemical & Engineering Data*, *59*(3), 850–859. https://doi.org/10.1021/je401002w

Kuriata, A., Gierut, A. M., Oleniecki, T., Ciemny, M. P., Kolinski, A., Kurcinski, M., & Kmiecik, S. (2018). CABS-flex 2.0: A web server for fast simulations of flexibility of protein structures. *Nucleic Acids Research*, *46*(W1), W338–W343. https://doi.org/10.1093/nar/gky356

Li, Y., Lin, Y., Garvey, C. J., Birch, D., Corkery, R. W., Loughlin, P. C., Scheer, H., Willows, R. D., & Chen, M. (2016). Characterization of red-shifted phycobilisomes isolated from the chlorophyll f -containing cyanobacterium *Halomicronema hongdechloris*. *Biochimica et Biophysica Acta (BBA) - Bioenergetics*, *1857*(1), 107–114. https://doi.org/10.1016/j.bbabio.2015.10.009

Ma, J., You, X., Sun, S., Wang, X., Qin, S., & Sui, S.-F. (2020). Structural basis of energy transfer in *Porphyridium purpureum* phycobilisome. *Nature*, *579*(7797), 146–151. https://doi.org/10.1038/s41586-020-2020-7

MacColl, R. (1998). Cyanobacterial phycobilisomes. *Journal of Structural Biology*, *124*(2–3), 311–334. https://doi.org/10.1006/jsbi.1998.4062

Marks, D. S., Hopf, T. A., & Sander, C. (2012). Protein structure prediction from sequence variation. *Nature Biotechnology*, *30*(11), 1072–1080. https://doi.org/10.1038/nbt.2419

Mirkovic, T., Ostroumov, E. E., Anna, J. M., van Grondelle, R., Govindjee, & Scholes, G. D. (2017). Light absorption and energy transfer in the antenna complexes of photosynthetic organisms. *Chemical Reviews*, *117*(2), 249–293. https://doi.org/10.1021/acs.chemrev.6b00002

Mullineaux, C. W. (2008). Phycobilisome-reaction centre interaction in cyanobacteria. *Photosynthesis Research*, *95*(2–3), 175–182. https://doi.org/10.1007/s11120-007-9249-y

Patil, G., Chethana, S., Madhusudhan, M. C., & Raghavarao, K. S. M. S. (2008). Fractionation and purification of the phycobiliproteins from *Spirulina platensis*. *Bioresource Technology*, *99*(15), 7393–7396. https://doi.org/10.1016/j.biortech.2008.01.028

Planavsky, N. J., Asael, D., Hofmann, A., Reinhard, C. T., Lalonde, S. V., Knudsen, A., Wang, X., Ossa Ossa, F., Pecoits, E., Smith, A. J. B., Beukes, N. J., Bekker, A., Johnson, T. M., Konhauser, K. O., Lyons, T. W., & Rouxel, O. J. (2014). Evidence for oxygenic photosynthesis half a billion years before the Great Oxidation Event. *Nature Geoscience*, *7*(4), 283–286. https://doi.org/10.1038/ngeo2122

Punjani, A., Rubinstein, J. L., Fleet, D. J., & Brubaker, M. A. (2017). cryoSPARC: Algorithms for rapid unsupervised cryo-EM structure determination. *Nature Methods*, *14*(3), 290–296. https://doi.org/10.1038/nmeth.4169

Scarff, C. A., Fuller, M. J. G., Thompson, R. F., & Iadanza, M. G. (2018). Variations on negative stain electron microscopy methods: tools for tackling challenging systems. *Journal of Visualized Experiments*, *132*, 57199. https://doi.org/10.3791/57199

Scheres, S. H. W. (2012). RELION: Implementation of a Bayesian approach to cryo-EM structure determination. *Journal of Structural Biology*, *180*(3), 519–530. https://doi.org/10.1016/j.jsb.2012.09.006

Scholes, G. D., Fleming, G. R., Olaya-Castro, A., & van Grondelle, R. (2011). Lessons from nature about solar light harvesting. *Nature Chemistry*, *3*(10), 763–774. https://doi.org/10.1038/nchem.1145

Su, H.-N., Wang, Q.-M., Li, C.-Y., Li, K., Luo, W., Chen, B., Zhang, X.-Y., Qin, Q.-L., Zhou, B.-C., Chen, X.-L., Zhang, Y.-Z., & Xie, B.-B. (2017). Structural insights into the cold adaptation of the photosynthetic pigment-protein C-phycocyanin from an arctic cyanobacterium. *Biochimica et Biophysica Acta (BBA) - Bioenergetics*, *1858*(4), 325–335. https://doi.org/10.1016/j.bbabio.2017.02.004

Rohou, A., & Grigorieff, N. (2015). CTFFIND4: Fast and accurate defocus estimation from electron micrographs. *Journal of Structural Biology*, *192*(2), 216–221. https://doi.org/10.1016/j.jsb.2015.08.008

Stewart, A., & Grigorieff, N. (2004). Noise bias in the refinement of structures derived from single particles. *Ultramicroscopy*, *102*(1), 67–84. https://doi.org/10.1016/j.ultramic.2004.08.008

van Stokkum, I. H. M., Gwizdala, M., Tian, L., Snellenburg, J. J., van Grondelle, R., van Amerongen, H., & Berera, R. (2018). A functional compartmental model of the *Synechocystis* PCC 6803 phycobilisome. *Photosynthesis Research*, *135*(1–3), 87–102. https://doi.org/10.1007/s11120-017-0424-5

Wagner, T., Merino, F., Stabrin, M., Moriya, T., Antoni, C., Apelbaum, A., Hagel, P., Sitsel, O., Raisch, T., Prumbaum, D., Quentin, D., Roderer, D., Tacke, S., Siebolds, B., Schubert, E., Shaikh, T. R., Lill, P., Gatsogiannis, C., & Raunser, S. (2019). SPHIRE-crYOLO is a fast and accurate fully automated particle picker for cryo-EM. *Communications Biology*, *2*(1), 218. https://doi.org/10.1038/s42003-019-0437-z

World Bank; IFC; MIGA. 2016. *World Bank Group Climate Change Action Plan 2016-2020.* World Bank, Washington, DC. World Bank. https://openknowledge.worldbank.org/handle/10986/24451 License: CC BY 3.0 IGO

Xiong, J., & Bauer, C. E. (2002). Complex evolution of photosynthesis. *Annual Review of Plant Biology*, *53*(1), 503–521. https://doi.org/10.1146/annurev.arplant.53.100301.135212

Yi, Z.-W., Huang, H., Kuang, T.-Y., & Sui, S.-F. (2005). Three-dimensional architecture of phycobilisomes from *Nostoc flagelliforme* revealed by single particle electron microscopy. *FEBS Letters*, *579*(17), 3569–3573. https://doi.org/10.1016/j.febslet.2005.05.033

Zivanov, J., Nakane, T., & Scheres, S. H. W. (2019). A Bayesian approach to beam-induced motion correction in cryo-EM single-particle analysis. *IUCrJ*, *6*(1), 5–17. https://doi.org/10.1107/S205225251801463X

Zhang, Jun, Ma, J., Liu, D., Qin, S., Sun, S., Zhao, J., & Sui, S.-F. (2017). Structure of phycobilisome from the red alga *Griffithsia pacifica*. *Nature*, *551*(7678), 57–63. https://doi.org/10.1038/nature24278